Acta Cryst. (1999). A**55**, 246–257

X-ray multislice computation using the Moodie–Wagenfeld equations: divergent-beam pattern simulation in three-beam and six-beam Laue cases

P. Goodman[a]* and Linda Liu[b]

[a]*The University of Sydney, National Center for Electron Microscopy and Microanalysis, Sydney, NSW 2006, Australia, and* [b]*School of Physics, University of Melbourne, Parkville, Victoria 3052, Australia.*
E-mail: pgoodman@myriad.its.unimelb.edu.au

(*Received 2 February 1998; accepted 14 August 1998*)

Dedicated to Professor A. F. Moodie on the occasion of his 75th birthday

Abstract

Pattern simulations for three-beam and six-beam X-ray diffraction are presented using multislice calculations based on Moodie & Wagenfeld's formulation of the X-ray equations, which factorize Maxwell's equations into Dirac format, using circular-polarization bases. The results are presented in three forms: one-dimensional rocking curves, *Pendellösung* thickness fringes, and convergent/divergent-beam patterns of single-diffraction orders, using experience gained from CBED (convergent-beam electron diffraction) and LACBED (large-angle CBED) techniques developed for high-voltage electron diffraction transmission patterns. This latter and quite new technique displays the results in the most compact form. The acronym DBXRAD (divergent-beam X-ray diffraction) is used for these patterns. The optics required for these patterns has only recently become available for radiations up to Mo $K\alpha_1$ in energy and for limited angular divergences, but with capillary focusing currently undergoing rapid development these limits are likely to be extended. However, these simulations define critical angular ranges within reach of current designs. Simulations for light- and heavy-atom structures belonging to the enantiomorphic space-group pair $P3_121$ and $P3_221$ provide clear evidence of chiral interaction between radiation and structure, highlighting divergences from the use in structure analysis of the well studied CBED pattern symmetries. Mo $K\alpha_1$ and Ta $K\alpha_1$ wavelengths were used to minimize absorption for the two structures studied, an important factor owing to the large thicknesses (up to 20 mm) required.

1. Introduction

In making comparisons with high-energy electron diffraction (HEED), for which spin interactions may be neglected, for X-ray scattering, even with the simplest classical model of atomic scattering from a dipole oscillator, vectorial, or for three-dimensional transmission, tensorial fields are basic. Rather than regarding this as a nuisance, our aim is to show how this may be used to advantage in solving three-dimensional structures and in tackling the ubiquitous phase problem in X-ray diffraction. For a detailed description of the implementation of the Moodie & Wagenfeld (1975) equations in multislice format, the reader is referred to the earlier studies of Patterson, Davis & Goodman (1999) where tests on Si and one-dimensional polar compounds having the ZnS structure are given. The basic idea behind our calculations is to regard both momentum and circular polarization states of the photon as changed by scattering, so, for a three-beam interaction based on a reciprocal-space triangle, two coupled triangles are envisaged, coupled according to the diagram of Fig. 1. As seen, paths between polarization states not involving a momentum change are forbidden (dashed lines).

In the present paper, this method is taken a step further in specifically looking at chiral structures. It has long been debated as to whether any measurable effects could occur at X-ray wavelengths commonly used in structure analysis resulting from a chiral interaction between photons of X-ray wavelengths, comparable with the well known observations made routinely with visible light known as ORD and CD (optical rotary dispersion and chromatic dichroism), representing the real and imaginary – or absorptive – components of refractive index. These established optical techniques allow determination of handedness in single molecules or in crystal structures belonging to triclinic space groups such as $P2$, the most commonly found symmetry in protein structures. Although these same effects may be eventually demonstrated for harder radiations, the computational program required in the X-ray case is much more complicated than that commonly used in electron microscopy, requiring 360° scattering (the Laue–Bragg condition) to be implemented. As a first step, and perhaps of more fundamental interest in crystallography, is that of distinguishing enantiomorphic space-group pairs, the one remaining problem in space-group determination for X-ray diffraction not yet solved even by the Bijvoet method (Peerdman *et al.*, 1951; Bijvoet *et al.*, 1951).

ISSN 0108-7673

In the present case, choice of wavelength is critical. For structures consisting of light atoms only, softer X-rays such as Cu $K\alpha_1$ may suffice, but as the atomic number increases so too does the radiation energy required to produce observable dynamic effects without introducing too great an absorption. We have found that the structure-dependent absorption, the so-called 'anomalous' absorption, plays an important role in the overall required dynamic interaction, only the average or zero-order absorption term not contributing to structural distinction and becoming a major factor to be considered in obtaining useable intensities from thick crystals.

From the well tabulated atomic scattering factors, Mo $K\alpha_1$ and Ta $K\alpha_1$ wavelengths were chosen for the above reasons in the computations for the two structures α-quartz and $Os_5(CO)_{16}$, respectively.

Earlier, wedge-shaped crystals had been used to study the effect of polarization scattering in two-beam X-ray transmission on an unpolarized incident beam (Hart & Milne, 1968), using a Lang camera (Lang, 1962), which involves a moving table holding a wedge-shaped crystal, the results for one diffraction order being recorded as a function of thickness. Then, Hart & Lang (1965) observed the periodic fading and re-emerging of *Pendellösung* fringe amplitude with thickness, arising from the beating of the two frequencies expected from the two independent linear polarization states σ^+ and σ^-, using wedge-shaped crystals of Si and Ge. Following this, observations were made using linear polarized radiation incident at 45° to the two-beam scattering vector so that equal amounts of σ- and π-state radiation coherently related formed the input beam (Skalicky & Malgrange, 1972). These authors found that a periodic beating could be observed with a polarizer only in the incident beam. This observation immediately suggested that treatment of the whole scattering as two sets of coupled harmonic oscillators could greatly simplify future analyses of Laue-case fringes, an analysis in which the beating is treated by considering both momentum and polarization states as taking part in a coupled coherent system. This layout of the problem then allows simple extension to N-beam coupling with $N > 2$, the simplest being the three-beam case. This is the smallest N interaction in which the structure phases play a part.

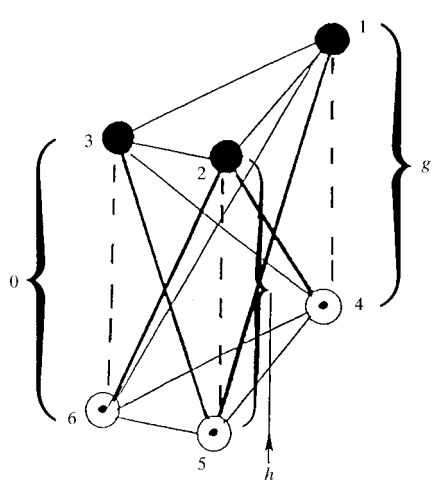

Fig. 1. The two three-beam momentum-scattering diagrams for circularly polarized X-rays, connected by allowed scattering paths to the opposite polarization state. Dashed lines represent forbidden paths, since polarization state cannot change without a scattering event. Beams collectively labelled 0, g and h represent reciprocal-lattice points that are split into σ^+ and σ^- states, denoted by filled and unfilled circles, numbered from 1 to 6 as shown.

The direct factorization of the whole transmission case as coupled equations for left and right circular polarization states (Moodie & Wagenfeld, 1975) then invited consideration of these cases, with the additional interest of exploiting the behaviour of circularly polarized states.

Until quite recently, however, an experimental method sufficiently sensitive to directly observe such weak effects as the chiral interaction between beam and structure from a simple diffraction experiment was lacking. The recent development and testing of capillary optics on a synchrotron source, which showed that a capillary focus could be used to produce divergent-beam elastically scattered diffraction orders using synchrotron radiation (Thiel *et al.*, 1989; Engström *et al.*, 1991; Bilderback *et al.*, 1994; Balaic *et al.*, 1996), prompted a fresh look at the Wagenfeld & Moodie equations, to examine the order of magnitude of three-dimensional X-ray scattering interactions of structural interest. The advantage of capillary optics is that, in principle, all the three-dimensional data could be collected from a single CBXRAD pattern from a single diffraction order. This concentration of incident energy into one pattern should help overcome the loss of energy in using both a polarizer (not necessary for synchrotron radiation) and an analyser in the detector path.

It may have been forgotten, or never properly appreciated, that prior to the Wagenfeld–Moodie publication (Moodie & Wagenfeld, 1975), the factorization of Maxwell's equations in Dirac-equation form was considered viable only for vacuum-state propagation (*e.g.* Sakurai, 1967), although there had been some theoretical effort put into presenting Maxwell's equations in spinor form for visible light (Hillion, 1979), but even there the accurate solution presented applies only to a medium of constant refractive index. However, with use of the multislice method, which treats the three-dimensional problem as a series of projected-structure phase gratings of zero thickness, and where all the propagation is in the vacuum state (Goodman & Moodie, 1974), it is made clear that this treatment is valid also in diffraction through a finite and periodically modulated refractive medium. Given that X-ray scattering amplitudes are an order-of-magnitude weaker than their electron-scattering counterpart, for which the

multislice method has already been thoroughly tested, the multislice treatment can be assumed to be very accurate for X-rays when fractional unit-cell slices are used, even for the heaviest atom.

2. Nomenclature

It is appropriate here to outline the differences adopted in X-ray and electron diffraction literature in their theoretical developments. Since the broad principles involved in the two subjects are the same, it is largely historical developments that have lead to independent formulations and nomenclature. This section may also be timely, since the most recent review by Weckert & Hümmer (1997) of multiple-beam X-ray diffraction uses the standard eigenvalue treatment for Maxwell's equations and deals almost exclusively with the determination of absolute configuration in organic compounds whose heaviest atom is nitrogen, and for as-grown crystals of 0.1 to 0.5 mm, and they are able to distinguish between use of anomalous absorption and use of three-beam interference as separate methods. With thick heavy-atom structures, this distinction is no longer possible; both phenomena are involved, and it is important that the anomalous-absorption coefficients for the atoms concerned be known to high accuracy.

For the present paper, we need to write the X-ray equations in the same form as the electron diffraction equations, and for this we propose a nomenclature for X-rays in the electron-equivalent form. We start by defining the interaction constant ε (rather than the normally used σ, to avoid confusion with its use for polarization state later in this paper), which, by multiplication with the appropriate structure factor, results in a scattering probability per unit length. Thus, $i\varepsilon_e\mathbf{VhZ}$ gives the kinematic (complex) scattering power per unit length for electrons, and $(\psi_h)_{\rm kin} = i\varepsilon_e\mathbf{V_h\Delta Z}$ gives the complex scattering amplitude in the first Born approximation, requiring $\varepsilon_e = 2/\mathbf{E}\lambda(1+\beta^2)^{1/2}$ (Cowley, 1981), with the appropriate relativistic term deriving from the Klein–Gordon equations. Here the electron difffraction structure factor $\mathbf{V_h}$ is expressed in volts, and $\mathbf{\Delta Z}$ is the thickness of a crystal slice. An expression for the complete Born series in the high-voltage limit ($\lambda \rightarrow 0$) is then given as $\psi_h = \exp(i\varepsilon_e\mathbf{V_h\Delta Z})$, the 'thin-phase-grating' approximation (Cowley & Moodie, 1957), which approaches the exact solution in the limit $\mathbf{\Delta Z} = 0$. In a similar way, $i\varepsilon_x\mathbf{F_h}$ gives the kinematic (complex) scattering power per unit length for X-rays, requiring that $\varepsilon_x = r_c\lambda/\Omega$, where r_c = the classical electron radius and Ω is the unit-cell volume (Davis, 1994).

Then, $\psi_h = \exp(i\varepsilon_x\mathbf{F_h\Delta Z})$ for N-beam dynamic X-ray diffraction in the equivalent high-energy limit, although the required approach to the limit $\mathbf{\Delta Z} \rightarrow 0$ is reached for much greater $\mathbf{\Delta Z}$ values than for electron diffraction, since $\varepsilon_e \gg \varepsilon_x$, allowing the multislice to be used for far greater atomic weights than is the case for electron diffraction. Different approximations are required for electron and X-ray diffraction which relate both to the much larger values of excitation error which give significant scattering in the electron case, directly related to the very much higher values of refractive index encountered in HEED, and because much larger values of θ_B (the Bragg angle) prevail for X-ray diffraction, the approximation that equates θ_B to $\tan\theta_B$ can no longer be applied. The expression for excitation error, $\Delta k_h = k_0 - k_h$ in the linearized form is still applicable since $\Delta k \ll k_0$. However, the extinction distance, which is only defined unambiguously for the two-beam approximation, is given by the condition $\varepsilon_e\mathbf{V_h}T = \pi$ for intensity extinction, where T is the total crystal thickness, and has a similar form $l_h = \pi/\varepsilon_e\mathbf{V_h}$ and $l_h = \pi/\varepsilon_x\mathbf{F_h}$ in the two cases. The values, however, are very different owing to reasons given above ($\varepsilon_e \gg \varepsilon_x$). The excitation error derived from the Ewald-sphere construction, $\Delta k_h = \tan(\Delta\theta_B)/d_h$, applies, with $[\Delta\theta_B/\theta_B]_{\text{X-rays}} \gg [\Delta\theta_B/\theta_B]_{\text{electrons}}$. We express excitation error values ζ_h as $\mathbf{\Delta k}$, derived from $\pm\mathbf{\Delta k} = \pm\zeta_h/\tan(\theta_B)$. This is summarized in Table 1.

Treating Maxwell's equations as a vector form of the Schrödinger equation makes for a simpler physical understanding as well as simpler evaluation. The standard form of Maxwell's equations due to Lorentz does not lend itself to simple interpretation. The Schrödinger formulation leads naturally to Dirac-type factorization as two coupled linear differential equations, which in turn allows the great simplification of using the S matrix as an operator, by-passing the need to formulate Bloch-wave states in crystal space, which are never required when considering elastic scattering (Heisenberg, 1944; Sturkey, 1962; Moodie, 1972*a*). In dynamic X-ray scattering, this comes about by Dirac-style linearization of the second-order differential equation. The great value of this, however, lies in the ability to interpret these equations: Dirac's genius allowed him to relate these equations to electron and positron scattering; in a parallel way, Moodie realized that for X-rays the equations represented right- and left-handed circularly polarized states, σ^+ and σ^-. In the following sections, we use these symbols as abbreviations in referring to the two polarization states.

3. Computed one-dimensional rocking curves for α-quartz and $Os_5(CO)_{16}$

The first technique followed is that of a rocking curve, which may be obtained experimentally using an accurate goniometer.

Fig. 2 shows these curves for the two isostructural compounds α-quartz (SiO_2) and $Os_5(CO)_{16}$, using Mo $K\alpha_1$ and Ta $K\alpha_1$, respectively. Both compounds belong to the enantiomorphic space-group pair $P3_121$ and $P3_221$ and have three molecular groups rotated by 120° along the z axis to form a spiral. The cations (Si and

Os) occupy the 3(*a*) site in α-quartz (Wykoff, 1948) and 3(*a*) and 6(*c*) sites in $Os_5(CO)_{16}$ (Reichert & Sheldrick, 1977). The calculations were therefore made for three slices per unit cell, with each slice chosen to have the cation 3(*a*) sites central, from which the projected charge density is used in a 'thin-phase-grating' approximation (see §2). These results are shown in Figs. 2(*a*) and (*c*). For comparison, a second calculation was run for which one-unit-cell projections (giving the projected symmetry *p*3) were run, to distinguish the

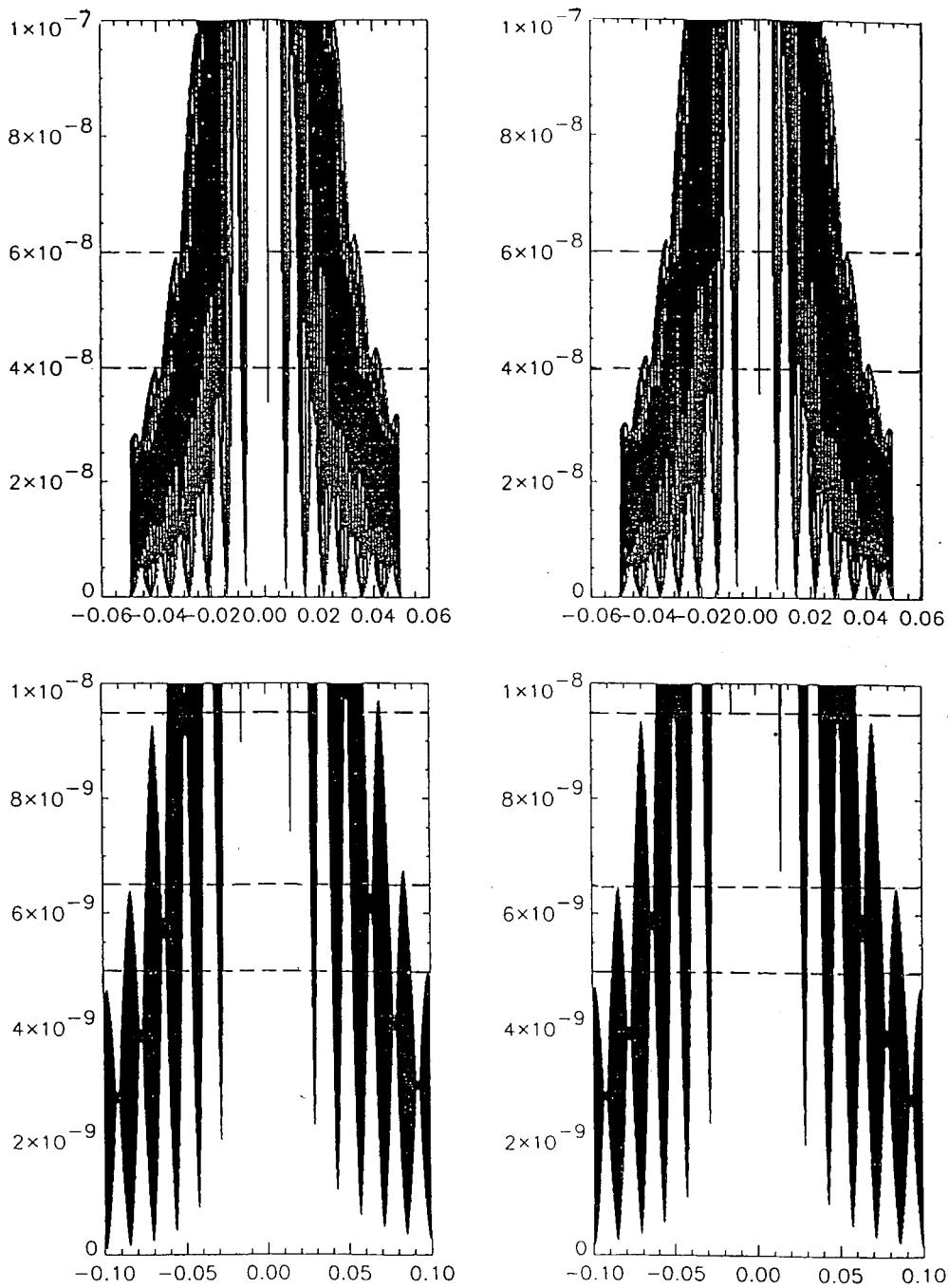

Fig. 2. Rocking curves obtained for α-quartz (upper curves) and for $Os_5(CO)_{16}$ (lower curves), for the $20\bar{2}0$ reflection in the symmetrical three-beam case for α-quartz using Mo $K\alpha_1$ radiation and for $Os_5(CO)_{16}$ using Ta $K\alpha_1$ radiation, respectively. Horizontal dashed lines at specific levels are a guide to the degree of asymmetry in the curves in the subsidiary maxima about the central peak. On the right side, the curves are simulated by the one-slice method (unit-cell projection), while those on the left side are simulated for the three-slice method, allowing chiral interaction along the *z* axis to be displayed.

Table 1. *Comparison between scattering terms for dynamic electron diffraction and dynamic X-ray diffraction*

Electrons	$\mathbf{V_h}$ (V)	$\varepsilon_e = 2\pi/E\lambda[1 + \frac{1}{2}(1 - \beta^2)^{1/2}]$	$l_h = \pi/\varepsilon_e V_h$
X-rays	$\mathbf{F_h}$ (electrons)	$\varepsilon_x = r_c\lambda/\Omega$	$l_h = \pi/\varepsilon_x F_h$

influence of three-dimensional chirality on the calculations. These results are shown in Figs. 2(*b*) and (*d*). The calculations here were run for 3×10^6 slices and 10^6 slices, respectively. To slice through these thicknesses within a reasonable time, a Cray computer was used. Thicknesses sufficiently great to show the three-dimensional interaction effects yet sufficiently small to prevent overriding absorption must be chosen. This amounted to depths of around 7 and 20 mm for SiO_2 and $Os_5(CO)_{16}$ using Mo $K\alpha_1$ and Ta $K\alpha_1$ wavelengths, respectively, for which 'anomalous-absorption' values χ_i' have been tabulated (Chantler, 1994).

Then, the left side of the diagrams in Figs. 2(*a*) and (*c*) show that the nonprojected chiral structures exhibit a much greater asymmetry across the rocking curves than do the projected structures of Figs. 2(*b*) and (*d*), increasing as the order of subsidiary maxima increases, as indicated by the horizontal dashed lines. Significantly, this asymmetry is just as noticeable for SiO_2 as for $Os_5(CO)_{16}$, showing that it is practical to use light-atom structures to obtain *N*-beam effects. The appearance of slight asymmetry in the one-unit-cell computed curves is due to the breakdown of the approximation $\tan(\Delta\theta_B) \approx \Delta\theta_B$.

4. Presentation of results in *Pendellösung* form

Presentation of the results in *Pendellösung* form, such as has been obtained in the past by use of the Lang camera (see §1) using a wedge-shaped crystal, permits us to obtain curves of diffracted intensities *vs* thickness, which give us a much more quantitative idea of the effect of chirality on intensities for different polarization states σ^+ and σ^-, and/or for the different symmetries $P3_121$ and $P3_221$. We should expect that if both are changed (say going from σ^+ radiation with $P3_121$ to σ^- radiation with $P3_221$), there would be no change in the transmitted diffracted intensities.

This proves to be the case in the calculations made. What we are looking at is either the ability to distinguish space groups $P3_121$ and $P3_221$ using fixed radiation states as input and selected output (by use of a polarization analyser), or to look at the effect of choosing different σ states on the same structure.

For the following wedge-shaped crystal *Pendellösung* simulations, we have chosen the orientation giving an equilateral triangle of diffraction points including the central beam and with either the $10\bar{1}0$, $1\bar{1}00$ or the $2\bar{2}00$, $20\bar{2}0$ reflection pairs as reflections *g* and *h*, numbered

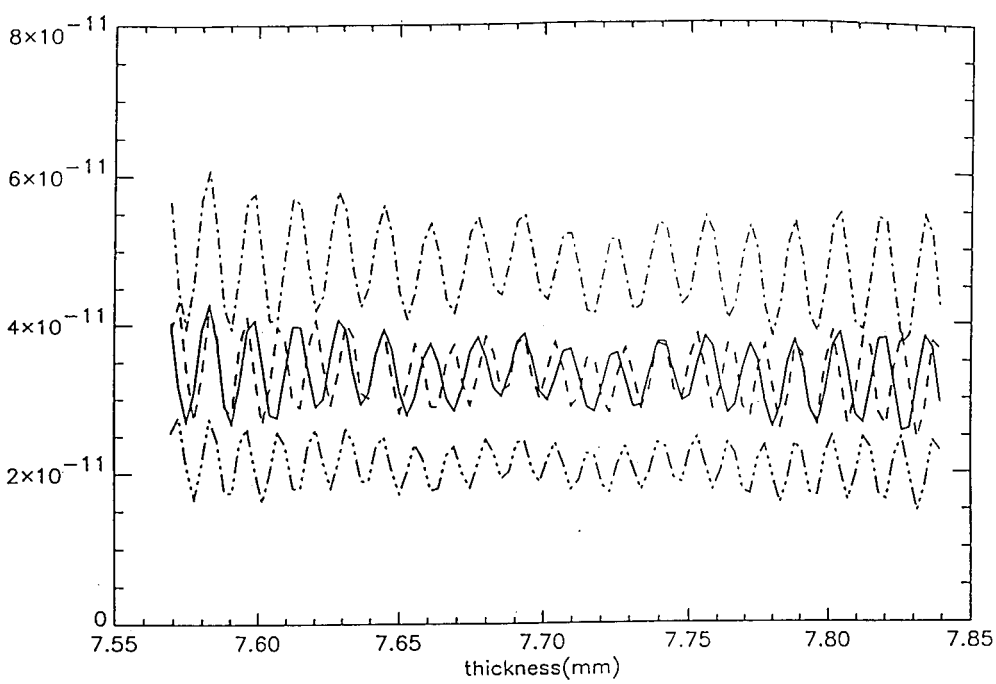

Fig. 3. Results for the three-beam case, 0000, $20\bar{2}0$ and $2\bar{2}00$ reflections, as a function of thickness for SiO_2 using Mo $K\alpha_1$ radiation. These curves are for the $2\bar{2}00$ reflection, showing the difference between the projection approximation, shown as a full line, and the full calculations, shown as broken lines. The central curves are for $\Delta k = 0$, while the upper and lower curves are for Δk values of $+0.3$ and -0.3, respectively.

beams 2 and 5, and 3 and 6 in Fig. 1. We use the *hkil* notation to avoid confusion when we compare the three-beam and six-beam calculations, with defined zone-axis coordinates [*uvwl*], rather than the shortened *hkl* notation. Fig. 3 shows the intensity of the $2\bar{2}00$ beam as a function of thickness for σ^+ radiation incident and σ^- transmitted, for the three-beam case involving 0000, $2\bar{2}00$, and $20\bar{2}0$ reflections for SiO_2 (α-quartz) using Mo $K\alpha_1$ radiation. These curves show the difference between computations for the projected structure (central curves) and those made for the full calculations, for Δk values of $\pm$ 0.3 for the space group $P3_121$.

Fig. 4 shows the different orientations used in the following work. Figs. 4(*a*) and (*b*) show the two three-beam excitations and Fig. 4(*c*) the six-beam interactions discussed.

Fig. 5 shows a calculation for $Os_5(CO)_{16}$ using Ta $K\alpha_1$ radiation. Here we see the effect of changing the sign of excitation error for Δk values of ± 0.1, exploring the asymmetry in the extended dynamic shape transform as in Fig. 3. For $Os_5(CO)_{16}$, we see a much greater difference from this asymmetry identifying chiral structures, and with a smaller deviation from θ_B, enhancing the ability to determine crystal hand. Admittedly, the thickness regime is greater, although intensity values on an absolute scale are not too different. Finally, six-beam simulations were run as shown in Fig. 4(*c*), in order to compare results with the three-beam simulation results. These were run firstly for the closest in reflection $2\bar{2}00$. The difference found in plots for the same calculation for the $2\bar{2}00$ triangle computed for only three beams was small, a slight drop in absolute intensity owing to energy being diverted into the other four diffracted beams. We saw from this that there is not much to be gained from a six-beam computation, at least for the close-in reflection. However, from trial calculations for the most distant reflection $6\bar{6}00$, we find that much better sensitivity can be gained by using small values for $|\Delta k|$, but at the cost of much reduced intensities. These preliminary results are therefore not given in this paper.

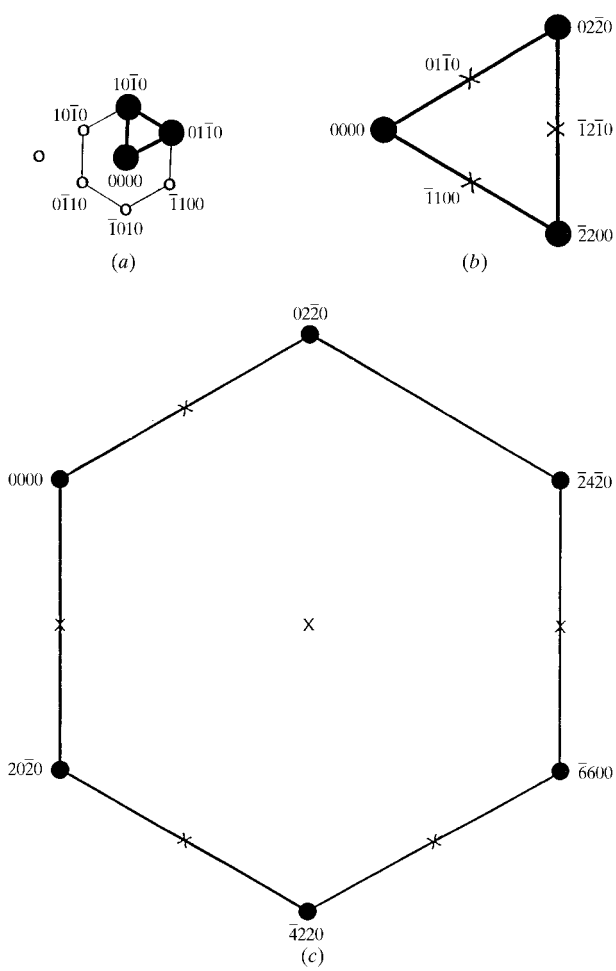

Fig. 4. Diagrams showing the orientations used for the three-beam and six-beam calculations. (*a*) Three-beam case for the $\{10\bar{1}0\}$ reflection set. (*b*) Three-beam case for the $\{02\bar{2}0\}$ reflection set. (*c*) Six-beam case, with the orientation shown, having the $01\bar{1}0$ reflection central in the hexagonal array.

5. DBXRAD patterns

5.1. *Methodology*

Until quite recently, the optics required for the DBXRAD technique was not available. The recent development and testing of capillary optics on a synchrotron source, which showed that a capillary focus could be used to produce convergent- and divergent-beam elastically scattered diffraction orders (Thiel *et al.*, 1989; Engström *et al.*, 1991; Bilderback *et al.*, 1994; Balaic *et al.*, 1996), however, allows us to make simulations for DBXRAD patterns with some chance of experimental testing. The great advantage of this technique is that the mechanical searching for precise *N*-beam orientions, which pushes the limit of feasibility and makes experiments tedious and difficult, is avoided. Use of approximate orientations would now suffice, given wide beam divergences of around 100 mrad, which will then cover the exact three-beam point somewhere in the diffraction disc in the three-beam case, and allows contemplation of the much more exotic aim of studying a six-beam interaction as in Fig. 3(*c*), only computed by the *Pendellösung* technique in this paper, with rather negative results. A future study by DBXRAD would not necessarily be so negative.

We chose thicknesses sufficiently great that the intensity fills as much of the aperture field as possible, with an aperture subtending approximately 90 mrad at the crystal for α-quartz, while for $Os_5(CO)_{16}$ this angle is 140 mrad. This corresponds to an excitation-error range of $\Delta k = 0.07$ for α-quartz, and of $\Delta k = 0.01$ for $Os_5(CO)_{16}$. These calculations were made for a thickness value of 10^6 unit cells, which, for calculations

involving slice depths of $1/3c$ (where c is the long unit-cell axis defined as the trigonal projection axis), gives a crystal thickness for α-quartz (Wykoff, 1948) of 0.54 mm, and, for $Os_5(CO)_{16}$ (Reichert & Sheldrick, 1977), a crystal thickness of around 2.5 mm.

These conditions have led to diffracted-beam intensities, expressed as fractions of the normalized incident beam taken as unity, of 10^{-7} to 10^{-8} for α-quartz and 10^{-8} to 10^{-9} for $Os_5(CO)_{16}$.

5.2. *Symmetries expected from DBXRAD patterns for space groups Nos. 152 and 154*

An examination of structure factors for the g and h reflections $101l$ and $110l$ for the enantiomorphs, using space groups Nos. 152 and 154 from *International Tables for Crystallography* (Hahn, 1987), abbreviated as ITA87, but using the structure-factor relationships only available in IT52 (Henry & Lonsdale, 1952), shows:

$$^{152}A_{hkl} = {}^{154}A_{hk-l}, \quad {}^{152}B_{hkl} = {}^{154}B_{hk-l}$$

and

$$^{152}A_{hkl} \neq {}^{154}A_{hkl}, \quad {}^{152}B_{hkl} \neq {}^{154}B_{hkl}.$$

This can be summarized as $^{152}F_{hk0} = {}^{154}F_{hk0}$ for the projected structure and

$$^{152}F_{hkl} = {}^{154}F_{hk-l} \tag{1}$$

for the upper and lower layer lines normally defined as having l integral, although non-integral values of l apply for points sampled at $\pm\Delta k$ of Moodie's dynamic shape transform (Moodie, 1972*b*) above and below the zero-layer reflections.

Further to this, in considering the first-order $10\bar{1}\bar{l}$ and $1\bar{1}0\bar{l}$ reflections, abbreviated to g and h reflections, we can derive the conditions

$$^{154}A_{hkil} = {}^{154}A_{hki-l} \quad \text{and} \quad {}^{154}B_{hkil} = {}^{154}B_{hki-l},$$

giving the conclusions

$$^{154}F_{hkil} = {}^{154}F_{hki-l} \quad \text{and} \quad {}^{152}F_{hkil} = {}^{152}F_{hki-l}. \tag{2}$$

Equations (1) and (2) will predictably lead to certain DBXRAD pattern symmetries provided the vector nature of the radiation is taken into account through use of the σ bases.

5.3. *Geometries to be avoided for chirality determination*

Eqations (1) and (2) introduce certain symmetries into the dynamic X-ray pattern. Reciprocity introduces additional symmetries dependent upon the existence of certain symmetry elements in the space group. Reciprocity involves a 180° rotation of the Ewald construction around the diffracting vector $\mathbf{\Delta k}$ (Moodie, 1972*b*). Mooodie's results relate to HEED. Figs. 6(*a*) and (*b*) show how reciprocity, which we now understand in terms of individual 'particle' states (Goodman & Gunning, 1992), behaves for photons as compared with HEED. Unlike HEED, using CBED, where these symmetries are useful in determining space group when detecting chirality and distinguishing its hand by means of specific pattern asymmetries with X-rays, we have to take the conditions producing these symmetries into account. They can be considered as conditions to be avoided as obscuring precisely the effects we wish to exploit.

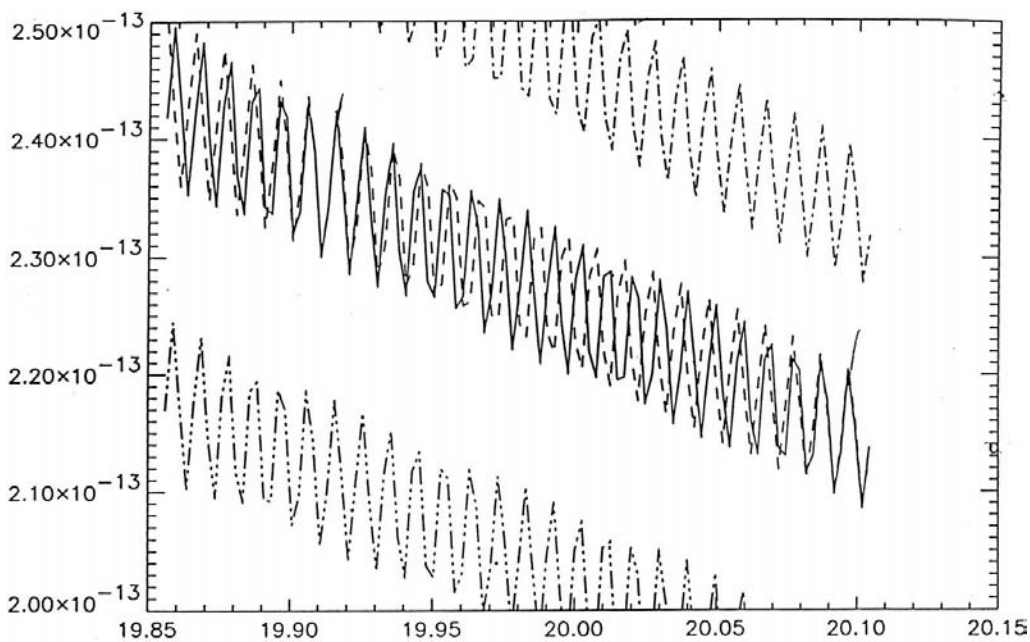

Fig. 5. Results similar to those of Fig. 3 for the $Os_5(CO)_{16}$ structure using Ta $K\alpha_1$ radiation and Δk_h values of ± 0.1.

Fig. 6(*a*) shows the reciprocity relationship as derived for electron diffraction, with the 180° rotation about **Δk** included. We have added to the $\mathbf{k}^{IN}$ and $\mathbf{k}^{OUT}$ vector polarization states, which are different for input and output beams, distinguished by dashed- and full-line arrows. The vertical Z axis is unique in that it is the propagation axis, but the sign choice is arbitrary; here we take Z as positive for the direction of the entrance-surface normal. In order to make the reciprocity relationship useable in the laboratory, we need to apply some symmetry element of the structure to invert the reciprocity ray paths. For space groups Nos. 152 and 154, we have twofold diad axes normal to **Z** (see figures on pp. 500 and 504 of ITA87), which when applied to this diagram produces the result shown in Fig. 6(*b*).

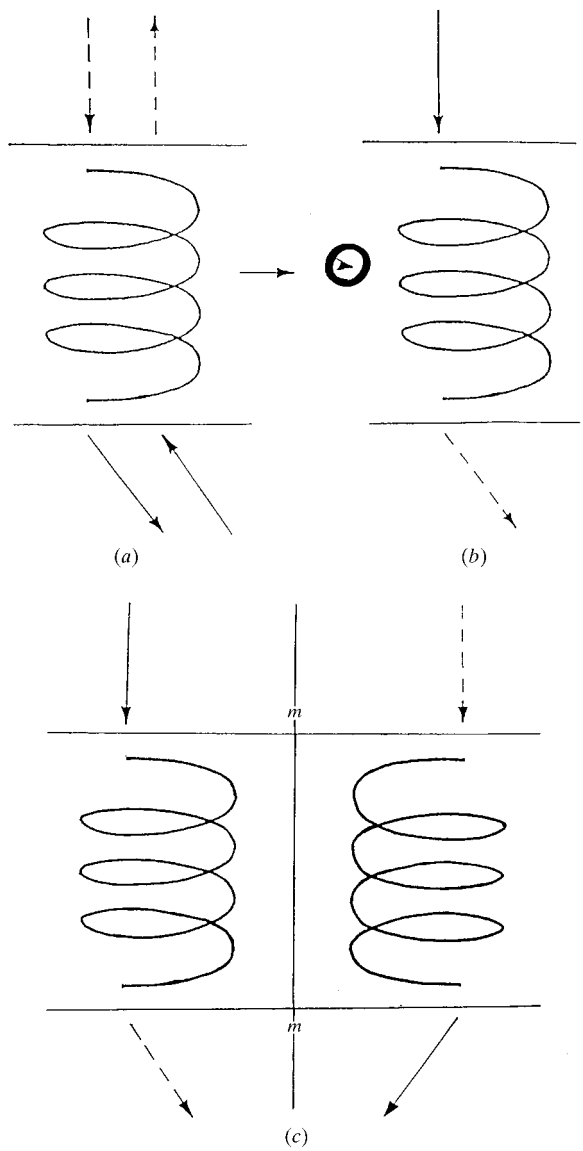

Fig. 6. (*a*) Diagram showing input and output beams, with full- and dashed-line arrows indicating different σ states, σ^+ and σ^-, respectively. (*b*) Diagram showing the two operations needed to (i) create the reciprocity diagram, indicated by a twofold rotation of 180° about the **Δk** vector (operator encircled), followed by a second twofold rotation, (ii) required to bring the reciprocally related beams into a realizable orientation for practical application in laboratory coordinates. (*c*) Diagram showing how a mirror reflection, which acts on the chiral crystal structure and input and output radiations, will give identical intensities for the transmitted beams.

This result implies that for a fixed space group, say No. 152 or 154, interchanging both the polarizer and analyser will result in identical intensity distributions in the analysed output beam and the DBXRAD patterns will be identical.

Another result is obtained directly without invoking reciprocity. Mirror-reflecting the whole diagram, which will mean reversing both the $\mathbf{k}^{IN}$ and $\mathbf{k}^{OUT}$ σ states as well as the structural handedness, will also yield identical intensities. This mirror effect is shown in Fig. 6(*c*).

A simple method of avoiding these conditions is to follow the momentum geometry of these diagrams with a fixed input polarization σ_1 and analyse for another fixed state σ_2. However, a more positive outcome is that, when the two symmetries shown in Fig. 6 are combined, we see that instead of changing the crystal hand in the beam, which would involve mounting a separate specimen, we can achieve the same result by exchanging only the σ states of input and output to obtain the same results, and hence examine the result of changing structural hand with the goniometer left in place.

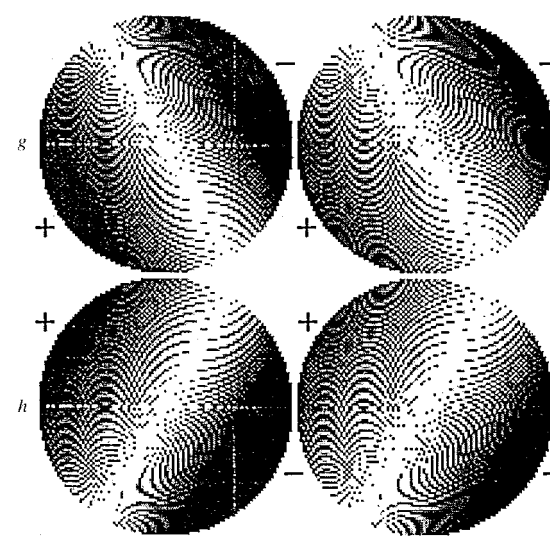

Fig. 7. Set of DBXRAD patterns, indicated as (*a*)–(*d*) in clockwise rotation from the upper left, showing results obtained for the average potential, using one slice per unit cell, for α-quartz with Mo $K\alpha_1$ radiation. (*a*), (*b*) and (*c*), (*d*) show the DBXRAD patterns for the $10\bar{1}0$ and $01\bar{1}0$ (*g* and *h*) reflections (upper and lower rows, respectively) for the symmetrical three-beam case of Fig. 4(*a*), with σ^+ incident and σ^+ and σ^- out. The columns in (*a*) and (*c*) are for σ^- out and the column of (*b*) and (*d*) are for σ^+ out. The labellings + and − on the disc edges indicate points for $+\mathbf{\Delta k}$ and $-\mathbf{\Delta k}$ values along the line normal to the bright central band for which $\Delta k = 0$.

5.4. *Results obtained by DBXRAD pattern simulations*

Figs. 7, 8 and 9 show three-dimensional diffraction intensity distributions in DBXRAD disc form, for beams g and h in the three-beam $0, g, h$ equilateral triangle, under different combinations of entrance and exit radiations, and for differences between the enantiomorphs. These discs also show the effects of reversal of excitation error, for $\pm\mathbf{\Delta k}$ values, which changes linearly (to a good approximation) along the trajectory normal to the central bright band and through its central Bragg point. The signs + and − at the disc edges indicate the two extreme ends of this trajectory, sampling the dynamic shape transform at equal distances above and below the Bragg point.

Fig. 7 shows results obtained for the projected α-quartz structure with Mo $K\alpha_1$ radiation, for which the single-unit-cell projection is used for the slice thickness with vacuum propagation between slices, to 0.54 mm thickness. Notable here is the exact mirror relationship shown between the g and h beams for both σ^+ and σ^- output (with σ^+ input), labelled states 2 and 3, and 4 and 5 according to Fig. 1. This calculation shows that without handedness we obtain the symmetry $P31m$ by effectively computing for only the zero-layer reflections $10\bar{1}0$ and $1\bar{1}00$ [see also equation (2) above]. Note that this leads to a translational relationship between the beams in horizontal rows, *i.e.* between the pair of beams g and h separately, when analysed for σ^+ and σ^- states (states 2 and 5, and 3 and 6, respectively, following Fig. 1).

Next, we made a simulation using 1/3 unit-cell slices and propagation between, to the same thickness, using a linear polarization at 45° to the set of g planes, which means that it can be either 15 or 75° to either the g or the h planes of the triangle. This follows the idea of Skalicky & Malgrange (1972), who were however using the two-beam case. The three-beam equilateral triangular geometry, however, has quite different symmetry properties to the one-dimensional two-beam interaction and this initial polarization mix gives rise to an imbalance in the clockwise and anticlockwise loops of cyclic geometry. This simulation is shown in Fig. 8 for α-quartz for the same crystal thickness and wavelength used for Fig. 9. What is noticeable here is the precise translational relationship between beam pairs 2 and 5, and 3 and 6, and, secondly, the breakdown of mirror symmetry between the g and h beams, 2 and 3, and 5 and 6.

These two features can now be interpreted directly. The translational relationship found in the two rows of discs can be understood from equation (2) above, showing the equality of points representing $+\mathbf{\Delta k}$ of g to $-\mathbf{\Delta k}$ of h. This relates directly to the situation found by reciprocity in HEED for identification of centrosymmetry (Goodman, 1975), making use of the reciprocity diagram given by Moodie (1972*b*).

Of interest here is the number of cyclic terms, corresponding to any path in a Moodie scattering diagram (Moodie, 1980–1985), which starts at 0 and follows the triangle in the order $0, g, h$ or $0, h, g$, being clockwise or anticlockwise depending on the choice of the positions of g and h in the triangle. We collectively call these cyclic terms. Terms that do not complete at least one circuit, leaving one side of the triangle empty, are called noncyclic. This is a diagramatic way of interpreting the Born series. With n as the order of each term, for $n = 3$ the cycle will finish at 0, so to finish at g with $n > 1$ and

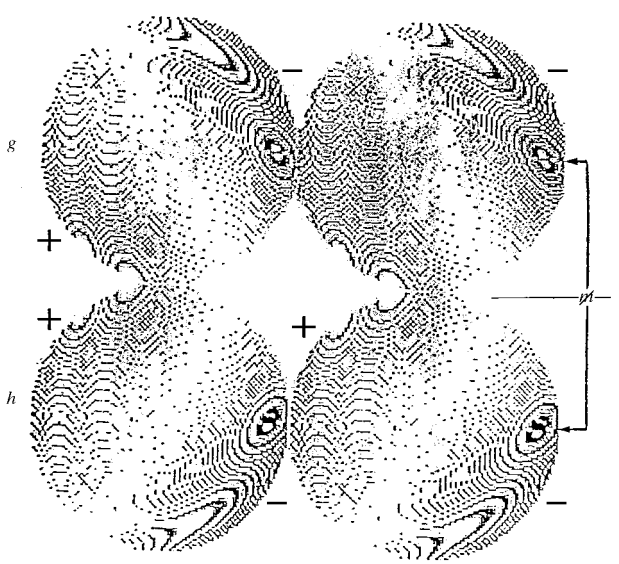

Fig. 8. (*a*) to (*d*), numbered and labelled in the same way and for the same three-beam case as in Fig. 7, show results obtained when using 45° linear polarization input (see text). The loss of exact mirror relationship is shown by arrows from the breakdown feature in the discs, using the symbol $\not m$ to indicate mirror breakdown.

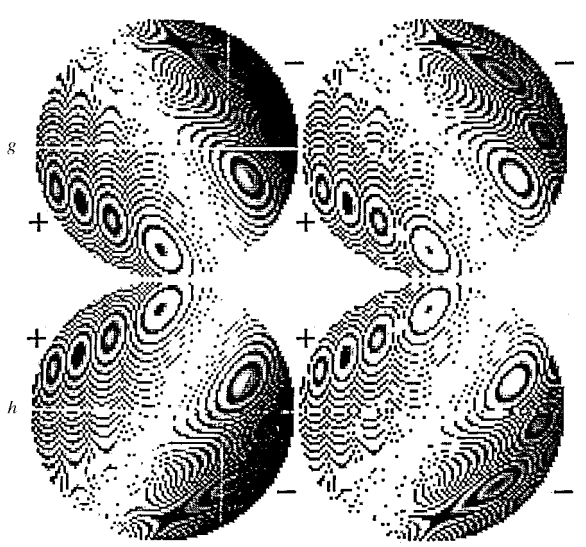

Fig. 9. DBXRAD results for the $Os_5(CO)_{16}$ structure and Ta $K\alpha_1$ radiation for the three-beam case with σ^+ incident and σ^+ and σ^- out, labelled in the same manner as in Fig. 7.

Table 2. *The Born series with cyclic terms that may be factored (see text)*

$n = 4$	$n = 5$	$n = 6$
$C\uparrow [A] + (B^3 + D)$	$C\uparrow [B + D] + (B^4 + A) + (A^3 + D^2)$	$C\uparrow [A^3] + (A^4 + BD) + (B^5 + D)$
$C\downarrow [A] + (B^3 + D)$	$C\downarrow [B + D] + (B^4 + A) + (A^3 + D^2)$	$C\downarrow [A^3] + (A^4 + BD) + (B^5 + D)$

$n = 7$

$C\uparrow\downarrow [A] + A^7 + (B^2 + A^5) + (A^5 + D^2) + (B^2 + D^2 + BD)$

$C\uparrow C\uparrow [A] + A^7 + (B^2 + A^5) + (A^5 + D^2) + (B^2 + D^2 + BD)$

$C\downarrow C\downarrow [A] + A^7 + (B^2 + A^5) + (A^5 + D^2) + (B^2 + D^2 + BD)$

gives the numerator terms in the Born series for n (without the $n!$ divisors) in the range $4 \rightarrow 7$, for multiple scatterings to g, where C represents cyclic paths of two classes, $C\uparrow$ and $C\downarrow$, for clockwise and anticlockwise triangular cycles, and $C\uparrow\downarrow$ represents a second-order cycle with both these superposed. Then A, B and D (rather than C, already in use) represent the three sides of the equilateral triangle, the *non*cyclic paths then being classified according to those paths along the sides of the triangle which are filled, and to what order. As $C^n = I$, the unit matrix, we have the series (after factoring out these unit matrix terms)

$n = 1$	$n = 2$	$n = 3$	$n = 4$	$n = 5$
A	$(BD)/2!$	$(A^3 + B^2A + AD^2)/3!$	$(A^2BD + BD^3 + B^3D)/4!$	$(A^5 + A^3D^2 + AD^4 + B^2A^3 + B^4A)/5!$

$n = 6$	$n = 7$
$(B^5D + B^3D^3 + BD^5 + A^3D^3)/6!$	$(A^7 + A^5D^2 + A^3D^4 + AD^6 + B^6A + B^4A^3 + B^2A^5)/7!$

$n = 8$	$n = 9$
$(B^7D + B^5D^3 + B^3D^5 + BD^7)/8!$	$(A9 + A^7D^2 + A^5D^4 + A^3D^6 + AD8 + B^6A^3 + B^4A^5 + B^2A^7)/9!$

representing the structure-factor component of the N-beam series for ψ_h, which must then include the excitation error series in ζ_h in order to give the result for ψ_h (Cowley & Moodie, 1962). For $n > 1$, the cross-product terms introduce a dependence on kinematic phase into the expression for ψ_h. The ratio m/p, where p is the total number of paths for a given n and m is the number cyclic paths, increases much more slowly than n, and unevenly, with jumps at each increase in power of C, so that the cyclic paths will tend to dominate at high n values (see text), the values for $n = 2, 3, 4, 5, 6, 7, 8, 9$ for the above ratio being $0/1, 1/6, 1/6, \underline{1/8, 2/10}, 2/13, \underline{2/10, 3/14}$ *etc*., showing this trend, with the *increased* terms of the series for $n > 2$ underlined to highlight this uneven and step-wise progress with n.

include these terms we must have $n > 3$. The ratio m/p, where m is the number cyclic terms and p is the total number of paths to g increases much more slowly than n, and in an uneven fashion, for $n = 2$, 3, 4, 5, 6, 7, 8, 9 the corresponding ratios m/p being $0/1, 1/6, 1/6, 1/8, 2/10, 2/13, 2/10, 3/14$ *etc*. Since for X-rays the complete Born series should be much more *rapidly* convergent than for electrons, this subset of the complete Born series could predictively lead to a detectable degree of chiral interaction between radiation and structure for sufficient thicknesses, as found in our simulations. As shown in Table 2, the cyclic paths may be factored out and behave as unit matrices of order 2, allowing factorization in terms of the Pauli matrices. This makes the influence of chirality more transparent.

It is a good idea in principle if we want to distinguish structural hand to give an imbalance at the entrance face by using the linear 45° state for one set of planes as noted above, since the initial conditions regarding phase are carried through several micrometres in transmission and must affect the end result even after several mm. This is one way of biasing either clockwise or anticlockwise cyclic paths, which with a pure σ^- or σ^+ entrance state would be in balance, and should lead to either enhanced or reduced interaction with a structure of particular hand. However, the results do not particularly show this to be the case, but do demonstrate that there is nothing to be gained by using pure σ states as compared with the linear 45° state as input.

Finally, in Fig. 9, we show the symmetries obtained for the $Os_5(CO)_{16}$ using Ta $K\alpha_1$ radiation for space group No. 152 for fixed σ^+ input and for both σ^+ and σ^- outputs. The most noticeable difference here from Fig. 8 is the obviously greater intensity displayed in the left-hand and right-hand diagrams – a feature of Fig. 8 was the evenness of both rows – the brighter of the beams in Fig. 9 being the σ^+ exit beams, or beams 2 and 3 for the double triangle. This illustrates that chiral interaction between radiation and structure will give enhanced transmission when both chiralities match (a not unexpected result). Apart from this, we have now lost the translational symmetry discussed above, but retained, to very good approximation, the mirror symmetry between the g and h rows. The only place where mirror breakdown can be seen is at the exact line of the bright and dark Kossel lines, which represents the trace of the condition for exact Bragg condition for the third beam. Actually, this is also the case in Fig. 9, but occupies much more prominence there.

The conclusion we draw from these results is that use of the heavy atom osmium is no help in detecting chiral effects by the DBXRAD method and that use of the experimentally simpler 45° of linear polarization as input is all that is required for the determination of crystal hand in this way.

6. Suggested experimental procedures

Because of the very weak beams we are examining in the CBXRAD technique and the requirement for polarized X-rays, synchrotron radiation was a natural choice for any experimental observation of the symmetry relationships we predicted by the above computations. Then, the technique described by Balaic *et al.* (1996) shows that, at least for soft X-rays (up to say the Mo $K\alpha_1$ wavelength), it is possible to produce a focus some mm from the exit of the capillary. This would allow space for the sample, controlled by a goniometer, and, as has been demonstrated by the above authors, this has produced disc-shaped diffraction orders at some distance from the sample at the focal point (or back-focal plane). In order to simulate the conditions of LACBED, we would also need to insert a circular aperture in the back-focal plane of such dimensions as to eliminate all diffuse scattering in neighbouring reciprocal space, and tightly define the particular diffraction order of interest. This has been effective in LACBED in eliminating almost all diffuse scattering from the required pattern structure consisting of Kossel- (or Kikuchi-) line and band detail, especially that due to TDS, which tends to be high-angle scattering. This would also be an essential component of any CBXRAD experiment, since we calculate only for elastically scattered X-rays, although with anomalous absorption included.

However, there are two problems with the type of focus achieved by the above authors. One is that the focus is highly concentrated around the directly transmitted ray and falls off rapidly across the disc from the centre outwards. In addition, we do not know how much of the initial linear polarization is retained by these capillaries. Another problem is that the type of glass used by them would not suit such hard radiation as Ta $K\alpha_1$; fortunately, we have demonstrated that the softer Mo $K\alpha_1$ radiation already tested with capillary focusing is all that is required for our purposes.

Bilderback *et al.* (1994) have suggested the use of lead glass for hard radiation, which carries with it an increased fluorescence from the capillary together with less-efficient central focusing. This fluorescence may in fact be a factor that would spread the radiation more evenly across the outgoing disc but would also lead to degradation of the polarization state. Clearly, more experimental work needs to be performed on testing different capillary designs to determine conditions most suitable for CBXRAD work.

It is interesting that, from what we have found from simulations, use of high atomic number elements, heavier than Si, does not help DBXRAD determinations, even though *Pendellösung* fringe results indicate enantiomorphic separation is greater for heavier material, which leaves open the possibility for examining even lighter atom structures such as organic compounds by the new method.

7. Discussion

The main conclusion we have reached is that enantiomorphic space-group pairs can be distinguished by means of dynamic single-crystal X-ray diffraction, and that a linearly polarized beam is all that is required. This latter conclusion was entirely unexpected when we started this investigation, but mature consideration has led us to believe that both theory and simulation, and hopefully experimental testing to follow, are at present in good agreement on this matter.

At a more basic level, there is an interest in the symmetrical three-beam problem in X-ray diffraction, long considered though not published (to our knowledge) by Professor A. F. Moodie (see however Moodie *et al.*, 1996). There is indeed some comparison to be made between this triangular scattering loop, which transmits σ^+ radiation much more strongly into the crystal of similar hand ($P3_121$) than σ^-, and the operation of a three-phase motor, which will only start in a particular direction. The difference here is essentially the difference between two- and three-dimensional problems.

Another question bound to be asked is, is this detection of chirality by X-rays purely abstract, considering that the same distinctions can much more readily be made with visible light? We are strongly of the opinion that this testing of phenomena known in the visible optics region in the X-ray wavelength region establishes important points in scattering theory, which we already feel assured will lead to other and better formulations of the dynamic theory of X-rays. Some of us (Goodman and Chantler) have started, as a consequence of the present work, on a new formulation for dynamic X-ray scattering.

Since this work has been contemplated for some years, we found that, before the present work, in any group of theoretical physicists in which this question was raised, the majority have said 'this will never work', while a minority have said 'the results will be positive but that is so obvious that it is not worth investigating'. It was this situation that led us to decide that it was worth going ahead with a relatively simple numerical test.

We would like to conclude on a positive note by paying tribute to the life-long and highly original personal theoretical thought put in by A. F. Moodie over a period of 40 years, which continues in 1998, and from whom those who were lucky enough to have him as supervisor for a period have learnt so much basic scattering physics. Typically of this scientist, most of his work was blackboarded as private discussion, and never published. We can only wish him a continuing and outstanding future.

We wish to acknowledge invaluable assistance from the following members of our School: Chris Chantler, Peter Paterson, Simon Matheson and Peter Dortmans in

particular who collaborated in unravelling problems of reciprocity and cyclic factorization.

Also, it is a pleasure to acknowledge the assistance given by one of the original authors of the Moodie–Wagenfeld theory, Hein Wagenfeld, who has sent us invaluable correspondence and papers relating to the chirality problem discussed here.

Last but not least, one of us (PG) wishes to acknowledge continuous encouragement throughout this project given by Geoff Opat and Tony Klein, the leaders of the 'Fundamental Experiments Group' within our School.

This research was partly funded by a Visiting Young Asian Scholarship awarded by Melbourne University.

References

Balaic, D., Barnea, Z., Nugent, K. A., Garret, R. F., Varghese, J. N. & Wilkens, S. W. (1996). *J. Synchrotron Rad.* **3**, 289–295.

Bijvoet, J. M., Peerdman, A. F. & van Bommel, A. J. (1951). *Proc. K. Ned. Acad. Wet. Ser. B*, **54**, 16–19.

Bilderback, D. H., Thiel, D. J., Pahl, R. & Brister, K. E. (1994). *J. Synchrotron Rad.* **1**, 37–42.

Chantler, C. T. (1994). *Resonant Anomalous Scattering – Theory and Applications*, edited by G. Materlik, C. J. Sparks & K. Fischer, pp. 61–78. Amsterdam: Elsevier Science B.V.

Cowley, J. M. (1981). *Diffraction Physics*, 2nd ed., p. 4. Amsterdam: North-Holland.

Cowley, J. M. & Moodie, A. F. (1957). *Acta Cryst.* **10**, 609–619.

Cowley, J. M. & Moodie, A. F. (1962). *J. Phys. Jpn*, **17**, Suppl. B-II, 86.

Davis, T. J. (1994). *Acta Cryst.* A**50**, 686–690.

Engström, P., Larssen, S., Rindby, A., Buttkewitz, A., Garbe, S., Gaul, G., Knöchel, A. & Lechtenberg, F. (1991). *Nucl. Instrum. Methods*, A**302**, 547–552.

Goodman, P. (1975). *Acta Cryst.* A**31**, 804–810.

Goodman, P. & Gunning, J. (1992). *Acta Cryst.* A**48**, 591–595.

Goodman, P. & Moodie, A. F. (1974). *Acta Cryst.* A**30**, 280–290.

Hahn, Th. (1987). Editor. *International Tables for Crystallography*, Vol. A. Dordrecht: Kluwer Academic Publishers.

Hart, M. & Lang, A. R. (1965). *Acta Cryst.* **19**, 73–77.

Hart, M. & Milne, A. D. (1968). *Phys. Status Solidi*, **26**, 185–189.

Heisenberg, W. (1944). Cited in: *Pions to Quarks: Particle Physics in the 50's*, edited by M. Laurie, M. Brown & M. Dresden. Cambridge University Press (1989).

Henry, N. F. M. & Lonsdale, K. (1952). Editors. *International Tables for X-ray Crystallography*, Vol. I. Birmingham: Kynoch Press.

Hillion, P. (1979). *J. Optics (Paris)*, **10**, 21–30.

Lang, A. R. (1962). *J. Phys. Soc. Jpn*, **18**, Suppl. 2, 332.

Moodie, A. F. (1972*a*). *Dynamical N-Beam Theory of Electron Diffraction. Encyclopedea Dictionary of Physics*, Suppl. 4, edited by R. G. Lerner & G. L. Trigg. New York: Addison-Wesley.

Moodie, A. F. (1972*b*). *Z. Naturforsch. Teil A*, **27**, 437–440.

Moodie, A. F. (1980–1985). Private discussions.

Moodie, A. F., Etheridge, J. & Humphreys, C. J. (1996). *Acta Cryst.* A**52**, 596–605.

Moodie, A. F. & Wagenfeld, H. (1975). *Acta Cryst.* A**31**, S249.

Patterson, D., Davis, T. J. & Goodman, P. (1999). In preparation.

Peerdman, A. F., van Bommel, A. J. & Bijvoet, J. M. (1951). *Nature (London)*, **168**, 271–272.

Reichert, E. & Sheldrick, G. M. (1977). *Acta Cryst.* B**33**, 173–175.

Sakurai, J. J. (1967). *Advanced Quantum Mechanics*, p. 169 (footnote). New York: Addison-Wesley.

Skalicky, P. & Malgrange, C. (1972). *Acta Cryst.* A**28**, 501–507.

Sturkey, L. (1962). *Proc. Phys. Soc.* **80**, 321.

Thiel, D. J., Stern, E. A., Bilderback D. H. & Lewis, A. (1989). *Physica (Utrecht)*, B**158**, 314–316.

Weckert, E. & Hümmer, K. (1997). *Acta Cryst.* A**53**, 108–143.

Wykoff, R. W. G. (1948). *Crystal Structures*, Vol. 1. New York: Interscience.